

How different are self and nonself?

Andreas Mayer,^{a,b} Christopher J. Russo,^{a,c} Quentin Marcou,^d William Bialek,^{a,e} Benjamin D. Greenbaum^{f,g}

^aJoseph Henry Laboratories of Physics and Lewis-Sigler Institute for Integrative Genomics, Princeton University, Princeton NJ 08544 USA

^bDivision of Infection and Immunity, University College London, London NW3 2PP, UK

^cProgram in Biophysical Sciences, The University of Chicago, Chicago IL 60637 USA

^dFaculté de Médecine La Timone, Aix-Marseille Université, 13005 Marseille, France

^eCenter for Studies in Physics and Biology, Rockefeller University, New York, NY 10065 USA

^fComputational Oncology, Department of Epidemiology and Biostatistics,

Memorial Sloan Kettering Cancer Center, New York, NY 10065 USA

^gPhysiology, Biophysics & Systems Biology, Weill Cornell Medicine,

Weill Cornell Medical College, New York, NY 10065 USA

(Dated: December 26, 2022)

Biological and artificial neural networks routinely make reliable distinctions between similar inputs, and the rules for making these distinctions are learned. In some ways, self/nonself discrimination in the immune system is similar, being both reliable and (partly) learned through thymic selection. In contrast to other examples, we show that the distributions of self and nonself peptides are nearly identical but strongly inhomogeneous. Reliable discrimination is possible only because self peptides are a particular finite sample drawn out of this distribution, and the immune system can target the “spaces” in between these samples. In conventional learning problems, this would constitute overfitting and lead to disaster. Here, the strong inhomogeneities imply instead that the immune system gains by targeting peptides which are very similar to self, with maximum sensitivity for sequences just one substitution away. This prediction from the structure of the underlying distribution in sequence space agrees, for example, with the observed responses to cancer neoantigens.

A basic task of the immune system is to distinguish self from nonself. More specifically, cytotoxic T cells should respond to relatively short peptides from foreign antigens and not respond to innocuous peptides, such as those synthesized by the organism itself. One might expect this task is easier in cases where peptide differences are larger, but recent work in cancer immunology has emphasized that cancer neoantigens which differ from self by just a single amino acid substitution can generate strong responses by the immune system. The strength of such recognition can exert a selective pressure on tumors, to which they adapt via mechanisms such as immune checkpoint signaling, the inhibition of which has been the basis of transformative immunotherapies [1–6]. T cells are, therefore, quite capable of recognizing peptides that are close to self. More generally, in the Immune Epitope Database [7] we find that nonself peptides which are one or two amino acids away from self peptides are more likely to be designated as immunogenic, while peptides with three or more amino substitutions are significantly less likely to generate an immune response (see Appendix A for details).

The distinction between self and nonself must be learned, at least to some extent, through the process of thymic selection. Because it is not possible for each candidate T cell to be tested against all possible self peptides, success requires some degree of generalization [8–12], as in all learning problems [13, 14]. We can think of examples as being drawn from a distribution, and in usual learning problems it is essential to capture features of this underlying distribution and not “overfit” to the particular random samples that one has seen. Perhaps surprisingly, we will show that the self/nonself distinc-

tion is in a different regime, where overfitting is both allowed and necessary. Our analysis allows us to understand why peptides that are very close to being self are natural targets for the immune system.

The structure of the self/nonself discrimination problem facing cytotoxic T cells is determined by the distribution of sequences found in the ~ 9 -mer peptides presented to the immune system by MHC class I. It is well known that the twenty amino acids are used with unequal probabilities [15], and it is easy to verify this by examining the entire human proteome, or the proteomes of large groups of infectious viruses or bacteria; for details of the databases we use see Appendix B. Correlations between neighboring amino acids are weak, but extend across a very long distance, far beyond the length of the relevant peptides. For k -mers with $k < 4$, the human proteome is large enough to sample all possible sequences, and we can estimate the probability distribution with reasonable control over errors. But there are too many possible 9-mers, and to say something about the underlying distribution requires building a model.

To describe the distribution of 9-mers, we adopt the maximum entropy framework [16]. The key idea is to build models that match particular features of the data exactly, but otherwise have as little structure as possible. This strategy has produced very accurate models for the joint patterns of activity in networks of neurons [17–19], correlated variations of amino acid sequences in protein families [20–24], fluctuating flight velocities in flocks of birds [25], and other problems. Importantly the maximum entropy method allows us to incorporate progressively more features of the data, incrementally, in search of a precise description. While the approach now is stan-

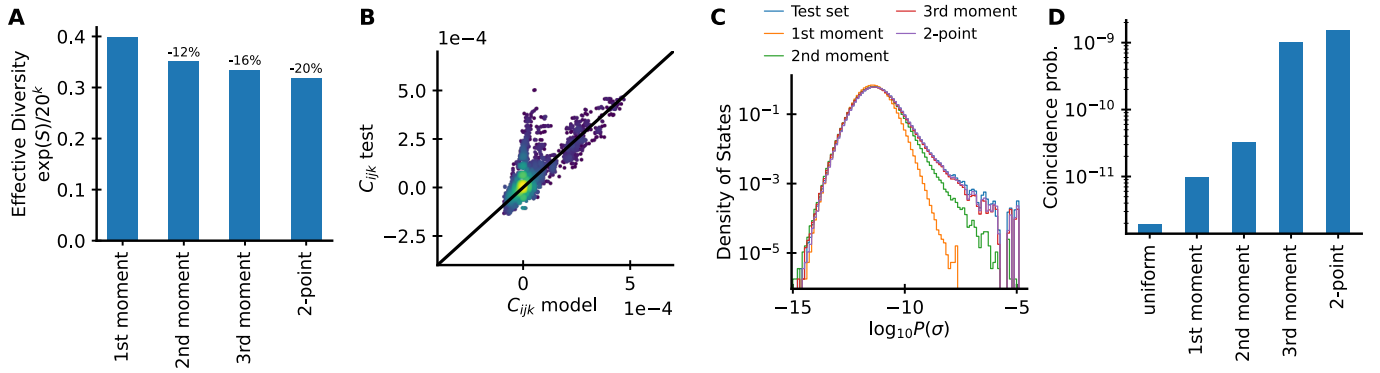


FIG. 1: **Maximum entropy model predicts peptide statistics.** (A) Entropy decreases as we add more constraints, corresponding to successive terms in Eq (2); see also Appendix C. (B) Predicted vs observed triplet correlations [Eq (4)] among amino acids at different sites. (C) Probability density of (log) probability in the full model. We compare ensembles of sequences drawn from the series of models in (A), and from the test set data. (D) Probability that two randomly chosen sequences are identical, computed across ensembles drawn from the series of models in (A).

dard, for completeness details are given in Appendix C.

Because correlations extend beyond the length of the 9-mers, we begin by matching global statistical features of these sequences: first the mean number of each type of amino acid that appears in the peptides, then the covariances in these numbers, and then their third moments. We can tell that each of these constraints is improving our model because each contributes to lowering the entropy, as seen in Fig 1A. Finally we include the fact that correlations between pairs of amino acids depend on the distance between them within the 9-mer.

Formally, we can define $s_i^\alpha = 1$ if the amino acid at site

i is of type α , and $s_i^\alpha = 0$ otherwise; $i = 1, 2, \dots, 9$ runs along the length of the peptide and $\alpha = 1, 2, \dots, 20$ as usual. We will refer to the entire sequence as $\sigma = \{s_i^\alpha\}$. It is useful to count the number of amino acids of each type that appear in the peptide, $n^\alpha = \sum_i s_i^\alpha$. With these definitions, the maximum entropy model described above takes the form

$$P(\sigma) = \frac{1}{Z} \exp[-E(\sigma)], \quad (1)$$

where the “energy”

$$E(\sigma) = \sum_{\alpha=1}^{20} \lambda_1^\alpha n^\alpha + \sum_{\alpha,\beta=1}^{20} \lambda_2^{\alpha\beta} n^\alpha n^\beta + \sum_{\alpha,\beta,\gamma=1}^{20} \lambda_3^{\alpha\beta\gamma} n^\alpha n^\beta n^\gamma + \frac{1}{2} \sum_{i,j=1}^9 \sum_{\alpha,\beta=1}^{20} J_\Delta^{\alpha\beta} s_i^\alpha s_j^\beta, \quad (2)$$

as explained in Appendix C. All of the coefficients must be adjusted so that the predictions of the model match observed features of the data: λ_1^α is fixed by matching the mean number of amino acids of type α ; $\lambda_2^{\alpha\beta}$ by matching the covariance in numbers of amino acids of types α and β ; $\lambda_3^{\alpha\beta\gamma}$ by matching the third moments of these numbers; the matrix $J_\Delta^{\alpha\beta}$, where $\Delta = |i-j|$, must be adjusted to match the distance dependence of the pairwise correlations; and the constant (partition function) Z serves to normalize the distribution, so that

$$Z = \sum_{\sigma} \exp[-E(\sigma)]. \quad (3)$$

We emphasize that once we match these measured features of the proteome, there are no free parameters that can be adjusted.

Does this family of models make accurate predictions

for higher order statistical properties of the human peptidome? As an example we can compute the correlations among triplets of amino acids at particular sites,

$$C_{ijk}^{\alpha\beta\gamma} = \langle \delta s_i^\alpha \delta s_j^\beta \delta s_k^\gamma \rangle, \quad (4)$$

with $\delta s_i^\alpha = s_i^\alpha - \langle s_i^\alpha \rangle$. All these correlations are very small but largely in agreement with the data (Fig 1B).

More subtly, the model assigns a probability of occurrence to every possible 9-mer, and we can calculate the distribution of this (log) probability, as shown in Fig 1C. As we constrain more features, this distribution grows a “heavy tail” of relatively high probability sequences that also is seen in the real data. To calibrate this effect, we note that there are nearly 10^{12} possible 9-mers, so the prediction that any sequences occur with probability above 10^{-7} reflects a startling 10,000-fold enrichment over random sequences, and many of these sequences are

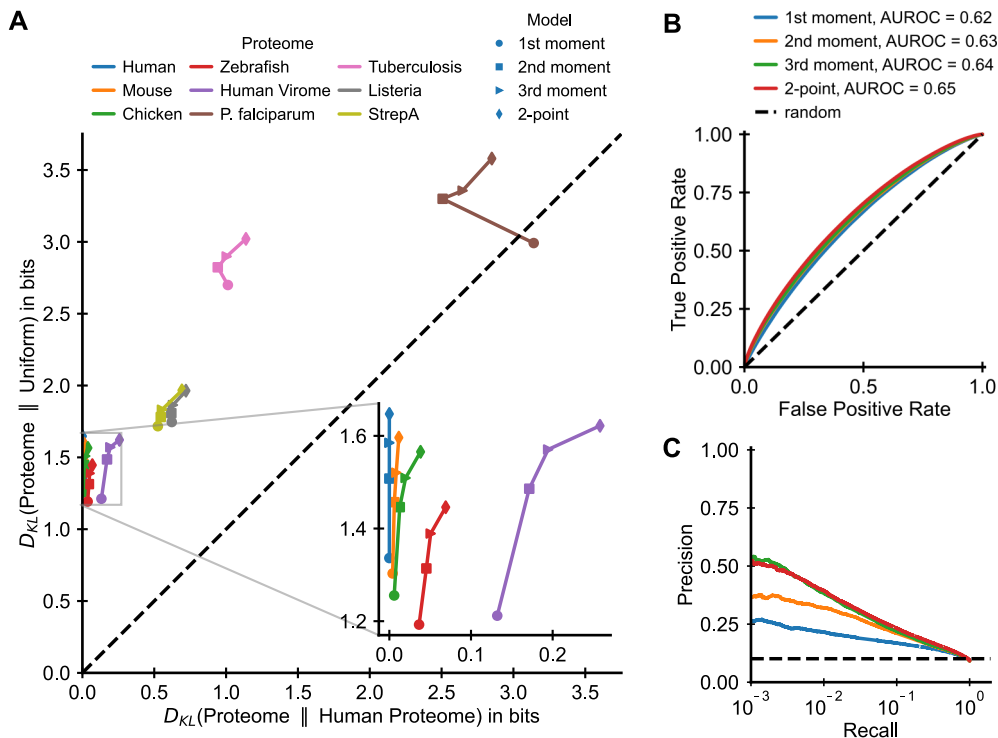


FIG. 2: Divergence between peptides from different proteomes. (A) Kullback-Leibler divergences between peptide distributions of different pathogen proteomes relative to human host peptides and relative to a uniform distribution over all peptides. For each proteome we show the statistical distance calculated according to a nested set of models including a different number of constraints. The inset shows a zoom on the set of proteomes close to the human statistics. (B, C) Performance of the models as classifiers, where we assign peptides as self or nonself based on the likelihood ratio $\mathcal{L} = \log[P_{\text{nonself}}(\boldsymbol{\sigma})/P_{\text{self}}(\boldsymbol{\sigma})]$ [26]. (B) If we choose a nonself peptide at random, there is some probability that it will be identified correctly (true positive), and if we choose a self peptide and random there is some probability it will be identified incorrectly as nonself (false positive). We can trade these probabilities against one another by changing the threshold \mathcal{L} at which we make the decision. (C) If self peptides are in $10\times$ excess, there is a probability that some random peptide will be classified correctly (precision), and this will “catch” a certain fraction of the nonself peptides (recall). Note that if peptides are assigned self/nonself at random, we will be right 10% of the time since self is in $10\times$ excess (dashed line).

found in the data. A corollary of this prediction, which will be very important for thinking about the immune response, is that two 9-mer sequences chosen at random are thousands of times more likely to be the same than expected if their individual amino acids were chosen at random (Fig 1D). Large effects on the coincidence probability coexist with relatively small effects on the entropy because the distribution is strongly non-uniform.

Having found a class of models that describes the distribution of 9-mer sequences quantitatively, we can ask whether this distribution differs between humans and other organisms, or between humans and pathogens. The natural measure of difference between distributions is the Kullback-Leibler divergence (D_{KL}), which measures the average evidence (or log-likelihood ratio) that a single peptide belongs to one distribution rather than the other [27]. Note that to evaluate this we need the partition function Z for each model, which we compute as described in Appendix D.

Figure 2A shows that all the distributions of 9-mers

are quite different from the uniform distribution, but quite similar to one another. As we add successive constraints expressed by the different terms in Eq (2), we find that not just amino acid frequencies, but also covariances are largely shared across proteomes. In particular, if we compare a collection of human viral proteomes with the human proteome, we have $D_{KL} \sim 0.2$ bits, so that individual 9-mers are on average almost indistinguishable. The largest divergence is found for the parasite *Plasmodium falciparum*, but this organism is known to have a very unusual AT-rich genome [28]. A consequence of the small D_{KL} is that if we try to recognize, for example, individual peptides from viruses, we can do this with high probability only if we are willing to accept a nearly comparable false positive rate, corresponding to autoimmunity (Fig 2B).

The tradeoff captured by the receiver operating characteristic in Fig 2B is independent of the overall probability with which we encounter self or nonself peptides. If, for example, there is a $10\times$ excess of self peptides, we

can calculate the probability that any one peptide will be identified correctly (precision), but we can trade this against the fraction of nonself peptides that will be recognized (recall). As shown by the precision versus recall curve in Fig 2C, even if we catch only one in a thousand nonself challenges—those which “stick out” as being most unlikely to occur in the self distribution—we still reach only $\sim 50\%$ chance of being right about a random peptide.

The usual regime for making distinctions is one in which examples are drawn from very different distributions, as with images of dogs and cats. It might be complicated to find the proper axes along which to measure these differences, but they are essential for reliable discrimination. Figure 2 shows that self/nonself discrimination is not in this regime; indeed, a good first approximation is that the distributions of peptides found in humans and pathogens are the same. Discrimination still is possible, but only because self peptides come from a fixed and finite sample even if the universe of pathogens is effectively unbounded. Exploiting the finiteness of the sample usually amounts to “overfitting” [13, 14], but for the immune system this is essential.

Because there are $\sim 10^{12}$ possible 9-mers, but only $\sim 10^7$ which are realized in the human proteome, the immune system can recognize pathogen sequences that fall into the spaces between self sequences even if they come from the same distribution. But these spaces are tight: if sequences were random, typical self peptides would be separated by only three amino acid substitutions. In fact the distribution is very inhomogeneous, as discussed above, so most of the spaces are even smaller.

We can make this geometric picture explicit by asking, for each 9-mer in an ensemble of human viruses, what is the distance to the nearest human sequence. As shown in Fig 3A, more than $\sim 0.1\%$ of these pathogenic sequences are identical with a human peptide, and more than 1% are just one amino acid away. These coincidences and near coincidences are 10 – 100 \times more frequent than expected if sequences were random, and captured almost perfectly by the model in Eqs (1, 2). The scale of these effects is biologically meaningful: the empirical coincidence probability of $\sim 10^{-3}$ implies that for a viral proteome with $\sim 10^4$ amino acids exact coincidences are common, whereas they would be rare in the absence of the biases captured in our model.

There are more viral sequences within one amino acid of a human sequence than perfect coincidences in part because there are $9 \times 19 = 171$ ways to be at distance one, but only one way to be at distance zero. Normalizing for this effect (Fig 3B), we see that the density of nonself sequences declines monotonically with distance from the nearest self sequence. Again this is very well described by our model of nonself sequences.

The model that we use here does not assume that viral sequences have evolved to mimic human sequences via molecular mimicry, but rather that they come from the same distribution, which might be simply because their

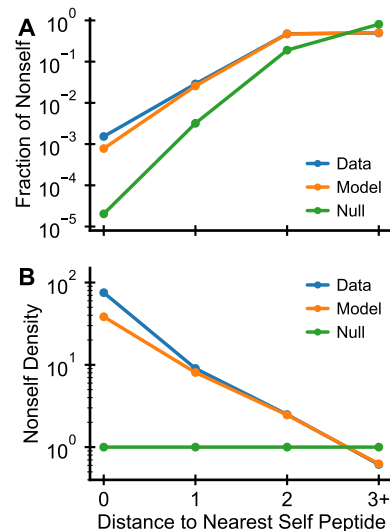


FIG. 3: **Many viral peptides are close to self.** (A) Distribution of distances to the nearest self peptide for peptides from human viruses as found in the data (cf Appendix B, blue), in predictions (orange) from the model in Eqs (1, 2), and in the null model with a uniform distribution over all 20^9 9-mers (green). (B) Relative density of viral peptides vs distance to the nearest human peptide. Colors as in (A).

proteins have the same physical constraints from the requirements of folding and function in host cells. We do see a small enhancement of exact coincidences above that predicted by the model, which might reflect some evolutionary pressure toward mimicry in specific cases. But even this phenomenon is made easier by the fact that most viral peptides start out only a few mutations away from self.

Taken together, these results lead to a “shell model” of immunogenicity, schematized in Fig 4. Because self and nonself peptides come from the same distribution, and this distribution is strongly inhomogeneous, targeting nonself peptides that are unlikely in the self distribution is unlikely to find anything. The highest density of nonself targets are in regions of sequence space where there is also the highest density of self peptides that must be avoided. To maximize the probability of hitting targets and avoiding self, the immune system should respond to peptides that are close to but not exactly self, and this preference should extend to those peptides that are as close as possible to self. A correlate of the similar peptide distributions is that training on peptides from the self can guide targeting of dense regions of nonself space, which provides a new perspective on the role of positive selection [29, 30]. Similarly, by overfitting to the relatively small set of “close to self” peptides, the immune system can leverage a small set of peptides to recognize a pathogen, providing a novel perspective on immunodominance, where indeed a relatively small peptide set

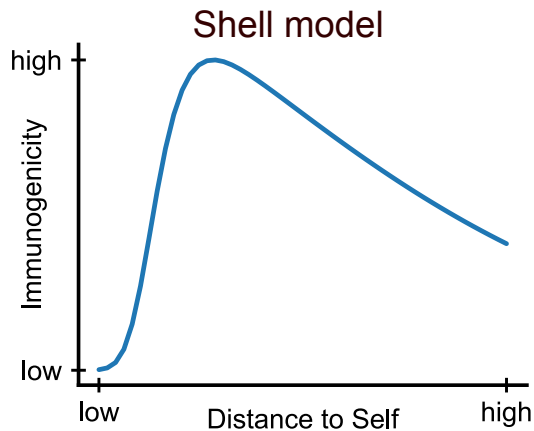


FIG. 4: **Schematic of the predicted biases in immunogenicity.** A shell model of nonself peptide recognition where the immune systems biases its search based on the more likely “close to self” peptides. Only (nearly) exact matches to self are non-immunogenic in this model due to tolerance.

drives immune responses. If we make assumptions about costs and benefits, we can turn the schematic of Fig 4 into quantitative predictions [31, 32]. Importantly, the

qualitative picture is independent of these assumptions: self and nonself are not very different, the distribution of these peptides is strongly inhomogeneous, and these results combine to mean that the immune system must target antigens close to those represented in the organism’s own proteome.

Acknowledgments

We thank Vinod Balachandran, Chrysothemis Brown, Curtis Callan, Warren James, Marta Łuksza, Taha Merghoub, Andrea Schietinger, and Zachary Sethna for insightful discussions. This work was supported in part by the National Science Foundation through the Center for the Physics of Biological Function (PHY-1734030); by a Lewis–Sigler fellowship (AM); by a Médecine Sciences fellowship of the Fondation pour la Recherche Médicale (QM); by fellowships from the Simons Foundation and the John Simon Guggenheim Memorial Foundation (WB); and by the Lustgarten Foundation, the Mark Foundation (ASPIRE Award), the NCI (P30CA008748, U01CA228963), the Pershing Square Sohn Foundation (Pershing Square Sohn Prize–Mark Foundation Fellowship), and Stand Up to Cancer (BDG).

-
- [1] H. Matsushita, M. D. Vesely, D. C. Koboldt, C. G. Rickert, R. Uppaluri, V. J. Magrini, C. D. Arthur, J. M. White, Y.-S. Chen, L. K. Shea, et al., *Nature* **482**, 400 (2012).
 - [2] T. N. Schumacher and R. D. Schreiber, *Science* **348**, 69 (2015).
 - [3] M. Łuksza, N. Riaz, V. Makarov, V. P. Balachandran, M. D. Hellmann, A. Solovyov, N. A. Rizvi, T. Merghoub, A. J. Levine, T. A. Chan, et al., *Nature* **551**, 517 (2017).
 - [4] A. Ribas and J. D. Wolchok, *Science* **359**, 1350 (2018).
 - [5] D. K. Wells, M. M. V. Buuren, K. K. Dang, T. N. Schumacher, P. Kvistborg, and N. A. Defranoux, *Cell* **183**, 1 (2020).
 - [6] M. Łuksza, Z. M. Sethna, L. A. Rojas, J. Lihm, B. Bravi, Y. Elhanati, K. Soares, M. Amisaki, A. Dobrin, D. Hoyos, et al., *Nature* **606**, 389 (2022).
 - [7] R. Vita, S. Mahajan, J. A. Overton, S. K. Dhanda, S. Martini, J. R. Cantrell, D. K. Wheeler, A. Sette, and B. Peters, *Nuc Acids Res* **47**, 339 (2019).
 - [8] T. C. Butler, M. Kardar, and A. K. Chakraborty, *Proc Natl Acad Sci (USA)* **110** (2013).
 - [9] F. P. Legoux, J.-B. Lim, A. W. Cauley, S. Dikiy, J. Ertelt, T. J. Mariani, T. Sparwasser, S. S. Way, and J. J. Moon, *Immunity* **43**, 896 (2015).
 - [10] W. Yu, N. Jiang, P. J. Ebert, B. A. Kidd, S. Müller, P. J. Lund, J. Juang, K. Adachi, T. Tse, M. E. Birnbaum, et al., *Immunity* **42**, 929 (2015).
 - [11] M. M. Davis, *Immunity* **43**, 833 (2015).
 - [12] I. M. N. Wortel, C. Kesmir, R. J. De Boer, J. N. Mandl, and J. Textor, *Cells* **9**, 690 (2020).
 - [13] P. Mehta, M. Bukov, C.-H. Wang, A. G. R. Day, C. Richardson, C. K. Fisher, and D. J. Schwab, *Phys Rep* **810**, 1 (2019).
 - [14] G. Carleo, I. Cirac, K. Cranmer, L. Daudet, M. Schuld, N. Tishby, L. Vogt-Maranto, and L. Zdeborová, *Rev Mod Phys* **91**, 045002 (2019).
 - [15] J. Lehmann, A. Libchaber, and B. D. Greenbaum, *J Theor Biol* **410**, 119 (2016).
 - [16] E. T. Jaynes, *Phys Rev* **106**, 1 (1955).
 - [17] E. Schneidman, M. J. Berry, R. Segev, and W. Bialek, *Nature* **440**, 1007 (2006).
 - [18] O. Moazo, G. Tkačik, M. Esteki, R. Kiani, and E. Schneidman, *Proc Natl Acad Sci (USA)* **117**, 25066 (2020).
 - [19] L. Meshulam, J. L. Gauthier, C. D. Brody, D. W. Tank, and W. Bialek, arXiv:2112.14735 [physics.bio-ph] (2021).
 - [20] A. Lapedes, B. Giraud, L. Liu, and G. Stormo, *Proceedings of the IMS/AMS International Conference on Statistics in Molecular Biology and Genetics* pp. 236–256 (1998).
 - [21] W. Bialek and R. Ranganathan, arXiv:0712.4397 [q-bio.QM] (2007).
 - [22] M. Weigt, R. A. White, H. Szurmant, J. A. Hoch, and T. Hwa, *Proc Natl Acad Sci (USA)* **106**, 67 (2009).
 - [23] D. Marks, L. Colwell, R. Sheridan, T. Hopf, A. Pagnani, R. Zecchina, and C. Sander, *PLoS One* **6**, e28766 (2011).
 - [24] S. Cocco, C. Feinauer, M. Figliuzzi, R. Monasson, and M. Weigt, *Repts Prog Phys* **81**, 1 (2018).
 - [25] W. Bialek, A. Cavagna, I. Giardinà, T. Mora, E. Silvestri, M. Viale, and A. M. Walczak, *Proc Natl Acad Sci (USA)* **109**, 4786 (2012).
 - [26] W. Bialek, *Biophysics: Searching for Principles* (Princeton University Press, 2012).

- [27] T. M. Cover and J. A. Thomas, *Elements of Information Theory* (Wiley, 1991).
- [28] W. L. Hamilton, A. Claessens, T. D. Otto, M. Kekre, R. M. Fairhurst, J. C. Rayner, and D. Kwiatkowski, *Nuc Acids Res* **45**, 1889 (2017).
- [29] N. Vrisekoop, J. P. Monteiro, J. N. Mandl, and R. N. Germain, *Immunity* **41**, 181 (2014).
- [30] B. Koncz, M. Balogh, B. T. Papp, L. Asztalos, L. Kemény, and M. Manczinger, *Proc Natl Acad Sci (USA)* **118** (2021).
- [31] A. Mayer, V. Balasubramanian, T. Mora, and A. M. A. Walczak, *Proc Natl Acad Sci (USA)* **112**, 5950 (2015).
- [32] A. Mayer, V. Balasubramanian, A. M. Walczak, and T. Mora, *Proc Natl Acad Sci (USA)* **116**, 8815 (2019).
- [33] A. Bonertz, J. Weitz, D.-h. K. Pietsch, N. N. Rahbari, C. Schlude, Y. Ge, S. Juenger, I. Vlodavsky, K. Khazaie, D. Jaeger, et al., *J Clin Invest* **119**, 3311 (2009).
- [34] Uniprot-Consortium, *Nuc Acids Res* **49**, 480 (2021).
- [35] D. H. Ackley, G. E. Hinton, and T. J. Sejnowski, *Cog Sci* **169**, 147 (1985).
- [36] J. Marchi, E. A. Galpern, R. Espada, D. U. Ferreira, A. M. Walczak, and T. Mora, *PLoS Comp Biol* **15**, e1007282 (2019).

Appendix A: Epitope immunogenicity

The Immune Epitope Database (IEDB) contains a collection of experimental data about T cell activation assays in response to different peptides [7]. The experiments recorded in the database involve assays, such as the enzyme-linked immunosorbent spot (ELISpot) assays, in which T cells from a donor sample are cultured in the presence of an antigen. This allows assessing the frequency of antigen-specific T cells by counting how many cells activate in response to the antigen and secrete cytokines. The ability of an epitope to elicit an immune response as measured by such an assay is commonly called the immunogenicity of the epitope.

To perform our analyses we downloaded the full T cell reactivity dataset from IEDB (http://www.iedb.org/downloader.php?file_name=doc/tcell_full_v3.zip) on 2022/07/05. The database collates results from multiple different experimental techniques. To make the assessment of responses more comparable each entry is accompanied by a qualitative measure, of which we make use. We define an epitope as immunogenic if its qualitative score was in any of the different positive categories (“Positive,” “Positive-Low,” and “Positive-High”). Some epitopes were measured in multiple independent experiments. In such cases, we retained the consensus immunogenicity across the experiments. The database contains data for different host species (mostly human and mouse), and we restricted our analysis to human host responses. Additionally, we restricted our analysis to the targets of cytotoxic T cells, epitopes presented on MHC class I. MHC class I proteins can bind to peptides with a narrow distribution of lengths. We restricted our analysis to peptides of length 9 amino acids, which is the peak of the length distribution.

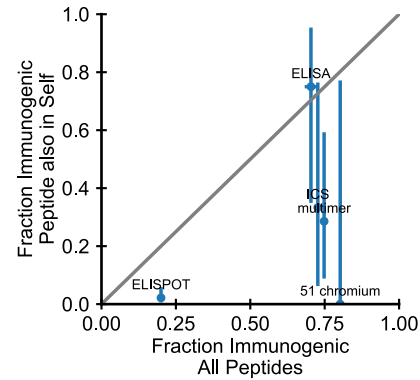


FIG. 5: **Different response frequencies between assays measuring immunogenicity.** Immunogenicity of foreign peptides with exact self matches versus immunogenicity across all foreign peptides. Assays vary in overall positivity rate, and relative positive response rates to peptides also found in self. The grey line shows equal response rates for visual reference. Assays: ELISPOT - enzyme-linked immune absorbent spot assay, ELISA - enzyme-linked immunosorbent assay, ICS - intracellular cytokine staining assay, multimer - pMHC multimer binding assay, 51 chromium - Chromium-51 release assay.

As we are interested in responses to pathogen-associated epitopes, we excluded epitopes annotated as coming from the host or of unknown provenance. We also excluded epitopes of foreign origin tested in the context of autoimmune disease, allergy, and cancer, as these might introduce a sampling bias towards “special” peptides close to self but immunogenic.

We next analyzed whether there were overall differences between different assay types represented in the database. We found that different assays differed greatly in the fraction of reported positives, and in the proportion of positive assays for foreign peptides with exact matches in the self-proteome (Fig 5). We consequently focus our further analysis on a single assay that accounts for the largest share of measured epitopes in the database (enzyme-linked immune absorbent spot assay), and which showed the smallest odds ratio between immunogenicity overall and for peptides with exact matches (Fig 5). The sensitivity of this assay to tolerance mechanisms is also supported by experiments demonstrating differential responses following depletion of regulatory T cells [33].

After these various filtering steps, we aligned all foreign epitopes to their nearest self-peptide by Hamming distance using an exact and fast hashing-based algorithmic approach. We then calculated the fraction of epitopes at different distances to self that are immunogenic (Fig 6). To assess statistical uncertainty in the fraction of immunogenic peptides, we calculate confidence intervals for the binomial proportions using the Jeffreys prior at a significance level of 0.1 as implemented in the Python package statsmodels v0.12.2.

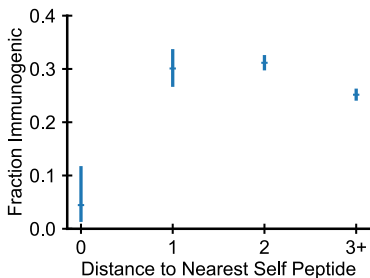


FIG. 6: Fraction of peptides of foreign origin that elicit a T cell response as a function of their Hamming distance to the nearest self peptide from the human reference proteome. Data: MHC class I epitopes of foreign origin from IEDB filtered as described in the text.

While epitopes identical to peptides found in the human proteome are less immunogenic, as expected, remarkably there are many epitopes that differ from self by a single amino acid which are immunogenic. Moreover, in contrast to some expectations, we found that the most dissimilar peptides (distance greater than 3) are recognized *less* frequently than those at intermediate distances from self. In summary, our analysis suggests the immune system naturally recognizes foreign epitopes close to self, even when farther peptides, more dissimilar from self, are available to be recognized. The same qualitative finding is also supported by a recently published, independent study [30], in which the analysis of epitope sequence similarity was restricted to T cell exposed motifs.

Appendix B: Human and pathogen sequences

We compared proteome statistics from model organisms across different branches of jawed vertebrates: human and mouse as two examples of mammals, chicken as an example of a bird, and zebrafish as an example of a jawed fish. We also compared them against a set of pathogen proteomes: a collection of human viruses (individual viral proteomes are too small for reliable statistical analyses), several pathogenic bacterial species (*Mycobacterium tuberculosis*, *Listeria monocytogenes*, and *Streptococcus pyogenes*), as well as a parasite (*Plasmodium falciparum*). These examples were chosen because of their representation in the database of immune responses (Appendix A). For each species we downloaded its reference proteome from Uniprot [34] using the proteome identifiers shown in Table I. The table also displays shortened names used in main text figure legends.

For the pan-viral proteome we downloaded all viral sequences annotated with human as a host species (taxon id: 9606) from Uniref90, a protein database clustered at 90% sequence identity.

For each proteome we then generated a list of all possible 9-mers by iterating over all possible starting posi-

tions within each protein from the proteome. We note that the total number of peptides is roughly equal to the total length of the proteome (except for forbidden start positions at the edges of the protein).

Appendix C: Maximum entropy models

We use the maximum entropy framework [16] as a principled way to include increasingly detailed statistical structure into a series of nested models for peptide statistics. Using this approach we constrain average features of the sequence $\langle f_\mu(\sigma) \rangle$ to equal their empirical values \bar{f}_μ , while otherwise keeping the probability distribution as random as possible. Mathematically, this means we choose a probability distribution that maximizes the Shannon entropy

$$S[P(\sigma)] = - \sum_{\sigma} P(\sigma) \log P(\sigma), \quad (\text{C1})$$

subject to the normalization constraint $\sum_{\sigma} P(\sigma) = 1$, and constraints that enforce the equality of modelled and empirical observables

$$\langle f_\mu(\sigma) \rangle = \sum_{\sigma} P(\sigma) f_\mu(\sigma) = \bar{f}_\mu. \quad (\text{C2})$$

Optimizing with respect to the normalization constraint yields a Boltzmann distribution of the form,

$$P(\sigma) = \frac{1}{Z} \exp[-E(\sigma)], \quad (\text{C3})$$

where

$$E(\sigma) = \sum_{\mu=1}^K \lambda_\mu f_\mu(\sigma), \quad (\text{C4})$$

is a sum of terms involving each constraint, and

$$Z = \sum_{\sigma} \exp[-E(\sigma)] \quad (\text{C5})$$

is a normalization factor, called the partition function. This is mathematically equivalent to the statistical mechanics of a system in thermal equilibrium, where $E(\sigma)$ is the energy as a function of its configuration.

Short name	Full name	Proteome ID
Human	Homo sapiens	UP000005640
Mouse	Mus Musculus	UP000000589
Chicken	Gallus gallus	UP000000539
Zebrafish	Danio rerio	UP000000437
Malaria	Plasmodium falciparum	UP000001450
Tuberculosis	Mycobacterium tuberculosis	UP000001584
Listeria	Listeria monocytogenes	UP000000817
StrepA	Streptococcus pyogenes	UP000000750

TABLE I: Reference proteomes used in estimating the distributions over peptides.

To fix the parameters λ_μ , we follow a standard method: At current values of the parameters we estimate $\langle f_\mu(\boldsymbol{\sigma}) \rangle$ using Monte Carlo sampling, then change parameters to reduce the discrepancy between estimated and empirical observables, and iterate until these discrepancies are nearly zero [35].

Correlations extend beyond the scale of peptides of interest, so we start by considering compositional constraints on the covariation of the total count of amino acids of different types. That is, we count the number of amino acids of each type in the peptide,

$$n^\alpha(\boldsymbol{\sigma}) = \sum_i s_i^\alpha, \quad (\text{C6})$$

and constrain its expectation value, and then do the same with the second and third moments

$$n^{\alpha\beta}(\boldsymbol{\sigma}) = n^\alpha(\boldsymbol{\sigma})n^\beta(\boldsymbol{\sigma}) = \left(\sum_{i=1}^L s_i^\alpha \right) \left(\sum_{j=1}^L s_j^\beta \right) \quad (\text{C7})$$

$$\begin{aligned} n^{\alpha\beta\gamma}(\boldsymbol{\sigma}) &= n^\alpha(\boldsymbol{\sigma})n^\beta(\boldsymbol{\sigma})n^\gamma(\boldsymbol{\sigma}) \\ &= \left(\sum_{i=1}^L s_i^\alpha \right) \left(\sum_{j=1}^L s_j^\beta \right) \left(\sum_{k=1}^L s_k^\gamma \right). \end{aligned} \quad (\text{C8})$$

This leads to a maximum entropy probability distribution with an effective energy

$$E(\boldsymbol{\sigma}) = \sum_{\alpha=1}^{20} \lambda_1^\alpha n^\alpha + \sum_{\alpha,\beta=1}^{20} \lambda_2^{\alpha\beta} n^\alpha n^\beta + \sum_{\alpha,\beta,\gamma=1}^{20} \lambda_3^{\alpha\beta\gamma} n^\alpha n^\beta n^\gamma. \quad (\text{C9})$$

This model only involves global couplings between amino acids independent of their distance.

Another common constraint involves the two-point frequencies $f_{ij}^{\alpha\beta}(\boldsymbol{\sigma}) = s_i^\alpha s_j^\beta$; the expectation value $\langle f_{ij}^{\alpha\beta} \rangle$ is the probability of finding amino acid of type α at site i and amino acid of type β at site j . By construction the data are translation invariant, except for edge effects arising from the finite length of proteins, so this should depend only on the distance $\Delta = |i - j|$ between the two amino acids. We explicitly enforce this invariance in the model by instead constraining the expectation value of

$$f_\Delta^{\alpha\beta}(\boldsymbol{\sigma}) = \frac{1}{2} \sum_{\substack{i,j=1 \\ |i-j|=\Delta}}^9 s_i^\alpha s_j^\beta. \quad (\text{C10})$$

Taking all these terms together, we end up with an effective energy (with $J_0^{\alpha\beta} = 0$)

$$E(\boldsymbol{\sigma}) = \sum_{\alpha=1}^{20} \lambda_1^\alpha n^\alpha + \sum_{\alpha,\beta=1}^{20} \lambda_2^{\alpha\beta} n^\alpha n^\beta + \sum_{\alpha,\beta,\gamma=1}^{20} \lambda_3^{\alpha\beta\gamma} n^\alpha n^\beta n^\gamma + \frac{1}{2} \sum_{i,j=1}^9 \sum_{\alpha,\beta=1}^{20} J_{i-j}^{\alpha\beta} s_i^\alpha s_j^\beta. \quad (\text{C11})$$

Appendix D: Calculating entropies and statistical divergences using thermodynamic integration

How can we determine the entropy of a fitted model? From the definition of the model in in Eq (1),

$$P(\boldsymbol{\sigma}) = \frac{1}{Z} \exp[-E(\boldsymbol{\sigma})], \quad (\text{D1})$$

we obtain the entropy

$$S[P(\boldsymbol{\sigma})] \equiv - \sum_{\boldsymbol{\sigma}} P(\boldsymbol{\sigma}) \log P(\boldsymbol{\sigma}) \quad (\text{D2})$$

$$= \langle E(\boldsymbol{\sigma}) \rangle_{P(\boldsymbol{\sigma})} - F, \quad (\text{D3})$$

where $F = -\log Z$. Similarly, we can express the Kullback-Leibler divergence as

$$D_{KL}[P(\boldsymbol{\sigma})||Q(\boldsymbol{\sigma})] = - \sum_{\boldsymbol{\sigma}} P(\boldsymbol{\sigma}) \log \frac{P(\boldsymbol{\sigma})}{Q(\boldsymbol{\sigma})}, \quad (\text{D4})$$

$$= \langle \Delta E(\boldsymbol{\sigma}) \rangle_{P(\boldsymbol{\sigma})} - \Delta F, \quad (\text{D5})$$

where $\Delta E = E_Q(\boldsymbol{\sigma}) - E_P(\boldsymbol{\sigma})$ and $\Delta F = F_Q - F_P$. In both instances, we can approximate the expectation

value over $P(\boldsymbol{\sigma})$ as the mean over Monte Carlo samples drawn from that distribution. But we also need to determine F , or the partition function of the fitted models.

As an exact evaluation of the partition function is computationally intractable we use thermodynamic integration to numerically approximate $F = -\log Z$ [36]: We define the perturbed energy function

$$E_g(\boldsymbol{\sigma}) = E_{\text{ref}}(\boldsymbol{\sigma}) + g\Delta E(\boldsymbol{\sigma}), \quad (\text{D6})$$

where $E_{\text{ref}}(\boldsymbol{\sigma})$ is a reference energy for which F_{ref} can be calculated analytically, and $0 \leq g \leq 1$ is a parameter scaling the additional energy term. For the maximum entropy model defined in Eq (2) we use

$$E_{\text{ref}} = \sum_{\alpha=1}^{20} \lambda_1^\alpha n^\alpha, \quad (\text{D7})$$

$$\begin{aligned} \Delta E(\boldsymbol{\sigma}) &= \sum_{\alpha,\beta=1}^{20} \lambda_2^{\alpha\beta} n^\alpha n^\beta + \sum_{\alpha,\beta,\gamma=1}^{20} \lambda_3^{\alpha\beta\gamma} n^\alpha n^\beta n^\gamma \\ &+ \frac{1}{2} \sum_{i,j=1}^9 \sum_{\alpha,\beta=1}^{20} J_{i-j}^{\alpha\beta} s_i^\alpha s_j^\beta. \end{aligned} \quad (\text{D8})$$

Notice that $g = 1$, $E_g(\boldsymbol{\sigma}) = E(\boldsymbol{\sigma})$ in Eq (2).

We have chosen E_{ref} to describe a model in which amino acids are chosen independently at each site, and we can see that

$$F_{\text{ref}} = -k \log \left[\sum_{\alpha=1}^{20} \exp(\lambda_1^\alpha) \right]. \quad (\text{D9})$$

In contrast, ΔE includes all couplings between different residues in the k -mer. Thus as we move along the family of models from $g = 0$ to $g = 1$, we interpolate between the independent model and the true model.

We can define the free energy F_g for the model at a specified value of the parameter g . Importantly, we have

$$\frac{dF}{dg} = -\langle \Delta E(\boldsymbol{\sigma}) \rangle_{P_g(\boldsymbol{\sigma})}, \quad (\text{D10})$$

where we emphasize again that the right hand side can be approximated as the mean over Monte Carlo samples. Thus we can calculate the free energy of the real model at $g = 1$ using “thermodynamic integration”

$$F(g = 1) = \int_0^1 dg \frac{dF}{dg} + F_{\text{ref}} \quad (\text{D11})$$

In practice, we draw Monte Carlo samples from the perturbed models with evenly spaced $g \in [0, 1]$, use these samples to evaluate dF/dg , and then evaluate the integral by Simpson’s rule.